Synthesis and High Performance of Magnetofluorescent Polyelectrolyte Nanocomposites as MR/Near-Infrared Multimodal Cellular Imaging Nanoprobes

Hyun Min Kim,[†] Hyunseung Lee,[‡] Kwan Soo Hong,[†,‡] Mi Young Cho,[†] Moon-Hee Sung,[§] Haryoung Poo,[⊥,*] and Yong Taik Lim[†,*]

[†]Graduate School and Department of Analytical Science and Technology, Chungnam National University, Daejeon 305-764, Korea, [‡]Division of MR Research, Korea Basic Science Institute, Cheongwon 363-883, Korea, [§]Department of Advanced Fermentation Fusion Science and Technology, Kookmin University, Seoul, and BioLeaders Corporation, Daejeon 305-500, Korea, and [⊥]Viral Infectious Disease Research Centre, Korea Research Institute of Bioscience and Biotechnology, Korea

ABSTRACT Here, we describe an easy but robust chemical strategy to synthesize high-performance magnetic resonance (MR)/near-infrared (NIR) multimodal imaging nanoprobes. Poly-(γ-glutamic acid) was used for the convenient phase transfer of $MnFe_2O_4$ nanoparticles dispersed in organic solvents into aqueous solutions and facilitated further ionic gelation with poly(L-lysine). During the gelation process, $MnFe_2O_4$ nanoparticulate satellites were encapsulated in the ionic nanocomplex, which induced synergistic magnetism and resulted in huge T_2 relaxivity (r_2). The positively charged outer surfaces were assembled with other negatively charged NIR emitting fluorescent nanocrystals and enabled the highly efficient delivery of the magnetofluorescent polyelectrolyte nanocomposites (MagFL-PEN) into cancer cells. The enhancement of negative contrast of MagFL-PEN at 2 μg/mL concentration was similar to that of Resovist at 20 μg/mL concentration. The NIR fluorescence microscopy images of the MagFL-PEN-labeled cells even at 12.5 pM were able to be clearly observed. The labeling efficiency of MagFL-PEN was approximately 65-fold higher compared to that of the commercialized fluorescent nanocrystals, only after 3 h incubation period, even at the test concentration (100 pM). Due to the high-performance capabilities both in materials properties and cell labeling efficiency, the MagFL-PEN is expected to be used as a highly efficient MR/NIR dual-modality imaging nanoprobe in the detection of cancer cells and monitoring of therapeutic cells *in vivo*.

KEYWORDS: imaging agents · nanostructures · polyelectrolyte · magnetic resonance imaging · near-infrared imaging · cancer cells

The development of molecular imaging nanoprobes with high resolution and high sensitivity capabilities is one of the key technologies for the early detection of diseases as well as an accurate understanding of basic biological processes. A variety of imaging nanoprobes have been developed in magnetic resonance imaging (MRI), positron emission tomography (PET), computed tomography (CT), and near-infrared (NIR) fluorescence imaging.[1−4] MRI is one of the best imaging tools for noninvasive *in vivo* imaging due to its high resolution, lack of exposure to radiation, superior soft tissue contrast, and long effective imaging window.[5−7] However, it has less sensitivity than nuclear medicine and fluorescence imaging to monitor small tissue lesions or molecular or cellular activities.[8,9] Several types of multimodal imaging nanoprobes, such as MRI/optical,[10−13] MRI/PET,[14,15] and PET/CT,[16,17] have been also developed using various chemical strategies in order to compensate for the inherent limitation of each imaging modality by the integration of quite conceptually different imaging techniques. Among various imaging modalities that can be combined with MRI, optical imaging technology is one of the best candidates due to its high sensitivity, cost-effectiveness, and use of nonradioactive materials. By the integration of the advantages of both MR and optical imaging techniques, the limitations of each technique (*e.g.*, the limited sensitivity of MRI, relatively less anatomic contrast information of optical imaging, and *ex vivo* information obtained with fluorescence microscopy) can be offset by other techniques.[18−20] In the case of optical imaging, considerable attention has been focused on the NIR fluorescence imaging technology, due to the relatively low absorbance and scattering of living tissue in the NIR region of the spectrum.[21−24] For MRI detection of magnetic nanoparticle (MNP)-labeled cells *in vivo*, several methods to maximize T_2 contrast effect with high relaxivity r_2 more than 200 mM^{-1} s^{-1} have been tried including

* Address correspondence to yongtaik@cnu.ac.kr, haryoung@kribb.re.kr.

Received for review August 1, 2011 and accepted September 20, 2011.

Published online September 20, 2011
10.1021/nn202912b

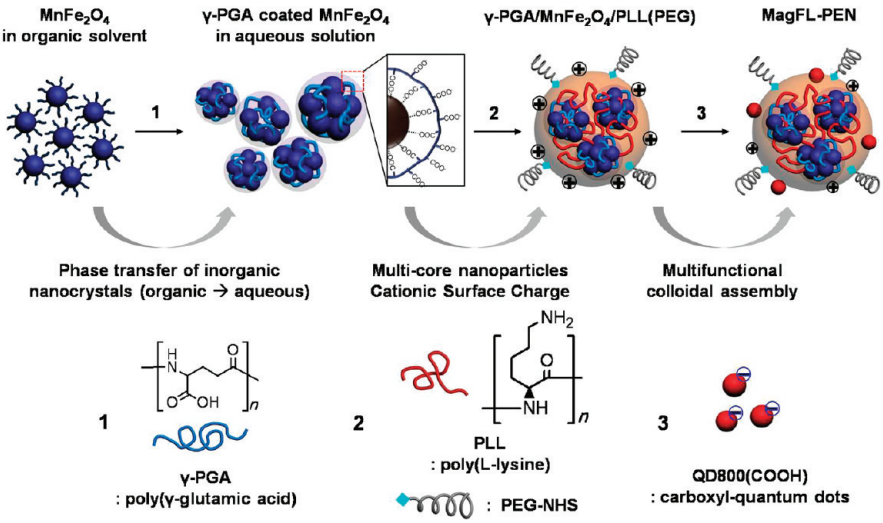

Scheme 1. Schematic illustration of the facile fabrication of MR/NIR multimodal imaging nanoprobes based on magneto-fluorescent polyelectrolyte nanocomposites (MagFL-PEN) *via* electrostatic assembly between polyelectrolytes and functional colloidal nanoparticles.

the following: (1) synthesis of ferrimagnetic MNPs,[25] (2) use of micrometer-sized particles,[26] (3) regulation of the number of cores in a particle,[27,28] (4) substitution of Fe by Mn in Fe_3O_4 cores,[29−31] and (5) fabrication of iron core-embedded ferrite MNPs.[32] Therefore, various strategies that can generate MR/NIR multimodal imaging nanoprobes having both high MR relaxivity and high optical sensitivity capabilities by robust and green chemistry are highly required in nanomedicine fields. To address these current issues, we have chosen an easy but robust chemical strategy to synthesize a high-performance MR/NIR dual-modality imaging (high relaxivity T_2-weighted MRI and highly sensitive NIR optical imaging) nanoprobe based on biocompatible polyelectrolytes, metal-doped multicore MNPs, and fluorescent nanocrystals and demonstrated their high performance in the multimodal imaging of cancer cells. The entire process mentioned above is very simple but robust for the generation of MR/NIR dual-modality nanoprobes reproducibly because most of the process is conducted in mild aqueous conditions using ionic interaction between polyelectrolyte materials and functional inorganic nanocrystals.[33−35] A schematic representation for the facile synthesis of polyelectrolyte nanocomposites as high-performance MR/NIR dual-modality molecular imaging contrast agents is shown in Scheme 1. Negatively charged polyelectrolytes containing a carboxyl group could be used for the convenient phase transfer of magnetic nanoparticles ($MnFe_2O_4$) dispersed in organic solvents into aqueous solutions and could facilitate further ionic gelation with positively charged polyelectrolytes. During the ionic gelation process, $MnFe_2O_4$ nanoparticulate satellites could be encapsulated in the ionic gel nanocomplex, which could induce synergistic magnetism and result in huge T_2 relaxivity (r_2). The positively charged outer surface could be assembled with other negatively charged NIR emitting fluorescent nanocrystals and could induce the highly efficient delivery of the magnetofluorescent polyelectrolyte nanocomposites (MagFL-PEN) into cancer cells.

RESULTS AND DISCUSSION

As a negatively charged polyelectrolyte, we have selected poly(γ-glutamic acid) (γ-PGA), which is a highly anionic polymer that has been suggested for use in a variety application such as food products, cosmetics, medicine, and so on.[36−39] γ-PGA is synthesized naturally by microbial species, most prominently by various bacilli, with an excellent biocompatibility and noncytotoxicity. γ-PGA-based nanoparticles have been used as a carrier for the oral delivery of insulin, employed to deliver protein vaccines, and appear to have a great potential as an adjuvant. Poly(L-lysine) (PLL) is a cationic biopolymer and has been known to be a nontoxic, biocompatible, and biodegradable with low immunogenicity and antibacterial properties.[40−42] Although more systematic evaluation on the toxicity of both polyelectrolytes is still required before clinical applications, they are already used in the medicine and food industries, which facilitates the biomedical applications of polyelectrolyte nanocomposites made by these two polyelectrolytes. The $MnFe_2O_4$ nanoparticles, which have the strongest MR contrast effect for T_2-weighted imaging among the several metal-doped superparamagnetic iron oxide (SPIO) nanoparticles, were synthesized by the thermal decomposition method for homogeneous and appropriate particle size (8 nm, Figure 1c). The $MnFe_2O_4$ nanoparticles are highly monodispersed in organic solvent such as hexane, toluene, and chloroform, as they are coated with a hydrocarbon chain of oleic acid and oleylamine.[43] Although $MnFe_2O_4$ nanoparticles synthesized in the organic phase have uniform size and morphology, their

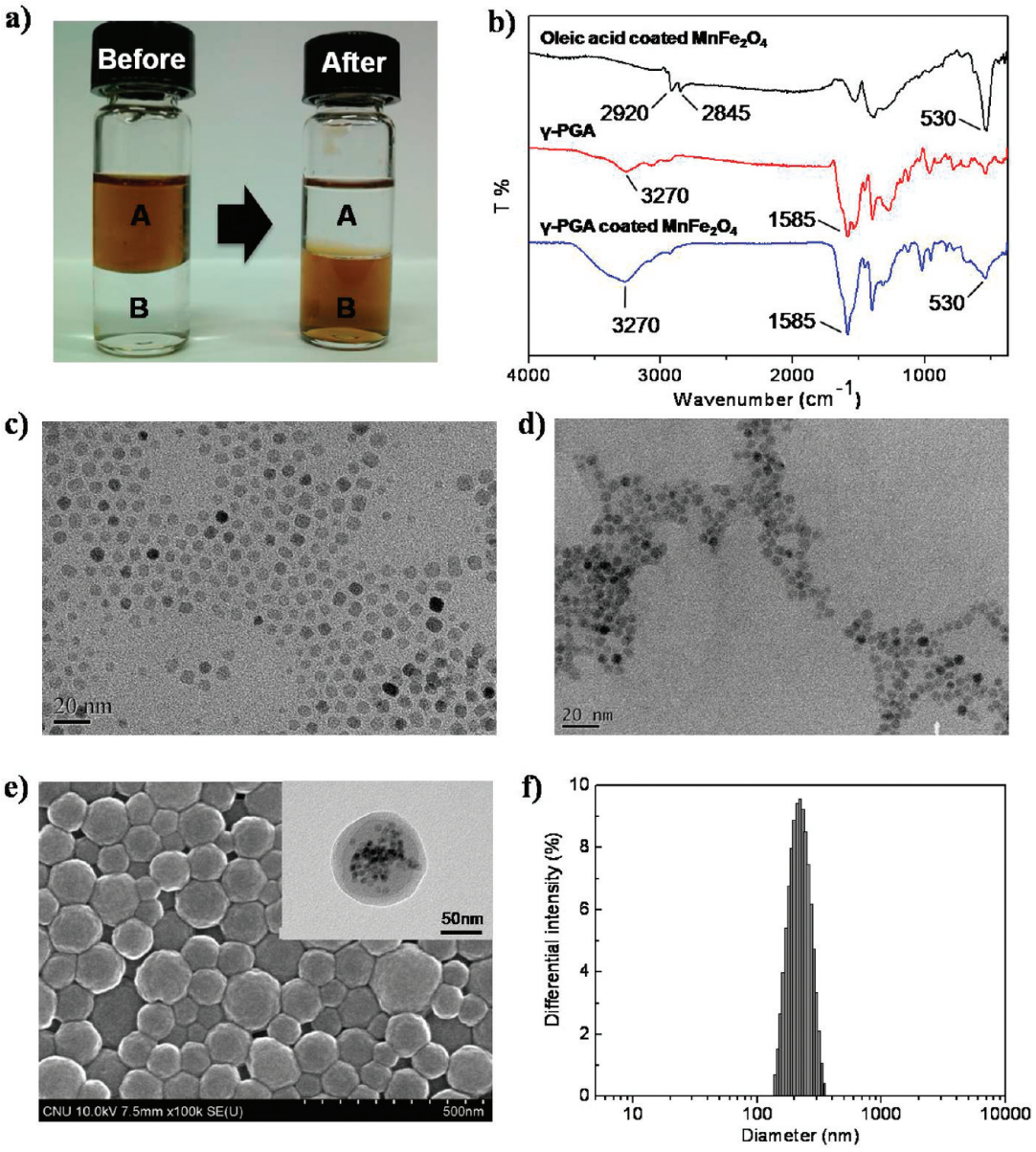

Figure 1. (a) Phase transfers of $MnFe_2O_4$ nanoparticles dispersed in hexane (A) into water after γ-PGA coating (B). (b) FT-IR spectra of oleic acid and oleylamine-coated $MnFe_2O_4$ nanoparticles, γ-PGA only and γ-PGA-coated $MnFe_2O_4$ nanoparticles. (c) TEM images of $MnFe_2O_4$ nanoparticles in hexane and (d) γ-PGA-coated $MnFe_2O_4$ nanoparticles in aqueous solutions. (e) SEM, TEM (inset) images, and (f) DLS analysis of γ-PGA/$MnFe_2O_4$/PLL(PEG).

surface should be changed or coated with a hydrophilic and biocompatible layer for *in vivo* biological application. To disperse these $MnFe_2O_4$ nanoparticles into aqueous solution, a phase transfer occurred by ligand exchange on the surface of $MnFe_2O_4$ nanoparticles between the hydrocarbon chain and γ-PGA. γ-PGA is a highly anionic polymer having a large amount of the carboxyl groups in their repeating sets. When the γ-PGA dissolved in DMSO was added into the $MnFe_2O_4$ nanoparticles dispersed in chloroform, abundant carboxyl groups along the γ-PGA chains approached the surface of $MnFe_2O_4$ nanoparticles, resulting in the ligand exchange between the carboxylic active site of γ-PGA and hydrocarbon molecules on the surface of nanoparticles.[44] Figure 1a demonstrates the success of $MnFe_2O_4$ nanoparticle surface modification by γ-PGA coating for phase transfer from organic solvent into the aqueous solution (50 mM $NaHCO_3$ solution, pH = 8.5). FTIR spectra (Figure 1b) also supported that the hydrocarbon ligand was successfully exchanged with γ-PGA. FTIR spectrum of oleic-acid-coated $MnFe_2O_4$ nanoparticles showed characteristic bands of oleyl chains at 2920 cm^{-1} (asymmetric C−H stretch), 2845 cm^{-1} (symmetric C−H stretch), and Fe−O vibration bands at 530 cm^{-1}. In the spectrum of γ-PGA-coated $MnFe_2O_4$, the Fe−O vibration bands still remained, while the C−H stretch bands of oleyl chains were removed. Moreover, new bands appeared at 3270 cm^{-1} (N−H stretch) and

1585 cm^{-1} ($-COO^-$ stretch), indicating that the surface of oleic-acid-coated $MnFe_2O_4$ was successfully modified by γ-PGA coating. TEM image of γ-PGA-coated $MnFe_2O_4$ (Figure 1d) shows that γ-PGA-coated $MnFe_2O_4$ nanoparticles intend to randomly suspend in aqueous solution rather than form a particulate structure. Up to now, various types of amphiphilic polymers or lipid molecules have been used for the surface modification of functional inorganic nanocrystals synthesized in organic solvents.[45−48] In this communication, the γ-PGA was first used for the convenient phase transfer of inorganic nanocrystals in organic solvents into aqueous solutions and provided numerous carboxyl moieties, which can facilitate the further ionic interaction with other positively charged polyelectrolytes and possible conjugation with biomolecules. When PLL were added into the γ-PGA-coated $MnFe_2O_4$ nanoparticles, PLL polymer chains formed an ionic gel complex with the nanoparticles by electrostatic interaction. Finally, poly(ethylene glycol) (PEG) was conjugated on the surface of γ-PGA/$MnFe_2O_4$/PLL nanogels. According to the SEM images (Figure 1e) and DLS (222.4 ± 42.3 nm) data (Figure 1f), we can see that the spherical shapes of γ-PGA/$MnFe_2O_4$/PLL(PEG) nanoparticles with narrow size distribution were successfully made. In TEM images (Figure 1e inset), it is confirmed that magnetic nanoparticles were encapsulated into a polymer matrix fabricated by ionic assembly between γ-PGA and PLL. Moreover, after complexing PLL with the γ-PGA-coated $MnFe_2O_4$ nanoparticles, a drastic change of ζ-potential from negative (−59.49 mV) to positive charge (+36.62 mV) was observed. The measured ζ-potentials of γ-PGA/$MnFe_2O_4$/PLL(PEG) nanogels from pH 5 to pH 10 are summarized in Table 1. Over pH 10.5 (known as pK_a of primary amine in PLL), the conversion of ζ-potential from positive to negative was observed, which resulted from the charge neutralization of PLL.

TABLE 1. ζ-Potential and Particle Diameter of γ-PGA/$MnFe_2O_4$/PLL(PEG) at Various pH Values

pH	5.2	6.6	7.7	8.3	10.6
ζ-potential (mV)	36.62	30.73	16.40	1.45	−20.03
average diameter (nm)	212.8	218.4	217.5	215.1	221.0

The positively charged outer surface can be further assembled with other negatively charged materials, such as carboxylic-acid-functionalized quantum dots (QD800(COOH)). Although we have used QD800(COOH)

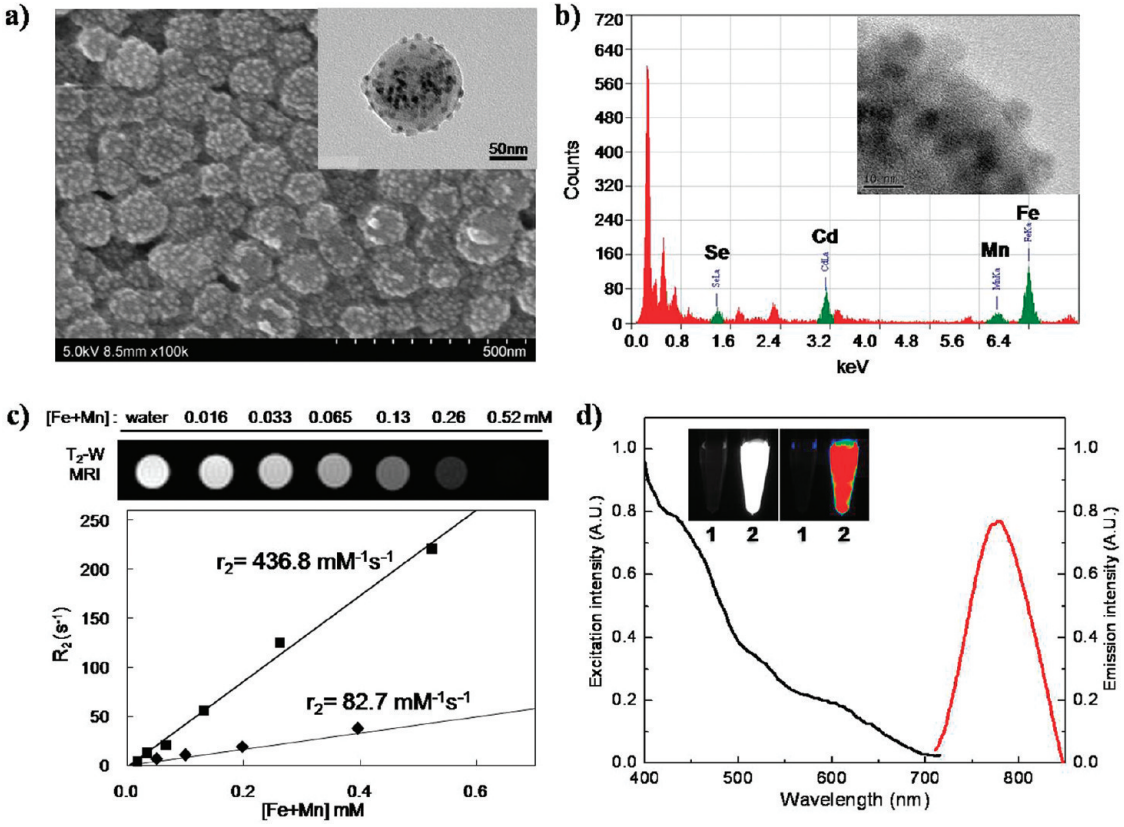

Figure 2. (a) SEM and TEM (inset) images of MagFL-PEN after adsorption of QD800(COOH). (b) EDX analysis of MagFL-PEN. (c) T_2-weighted (T_2-W) MR images and T_2 relaxation rates ($1/T_2$, s^{-1}) of MagFL-PEN (■) and γ-PGA-coated $MnFe_2O_4$ (♦) as a function of [Fe + Mn] concentration (mM) (4.7 T, 25 °C). (d) NIR excitation spectra (black) and emission spectra (red) of MagFL-PEN (inserted NIR fluorescence images (left) and their color map (right) of MagFL-PEN: (1) γ-PGA/$MnFe_2O_4$/PLL(PEG) and (2) MagFL-PEN.

TABLE 2. ζ-Potential Change and Particle Diameter of MagFL-PEN Solution at Different Concentration Ratio between QD800(COOH) and (Fe + Mn)

QD800nM(COOH) nM /(Fe + Mn) μg	0.16	0.32	0.64	1.28	2.56
ζ-potential (mV)	32.29	27.94	23.62	N/A	−14.53
average diameter (nm)	242.4	256.4	329.2	N/A	343.9

as a model of NIR emitting fluorescent nanocrystals in this study, other non-heavy-metal-based quantum dots and/or biocompatible organic dyes can be used as alternatives for future clinical applications.[49] To develop a high-performance MR/NIR dual-modality molecular imaging agent, we attached NIR emitting QD800-(COOH) to the surface of positively charged γ-PGA/$MnFe_2O_4$/PLL(PEG) nanogels. The addition of QD800-(COOH) (diameter = ~25 nm, λ_{em} = 775 nm, pH 9 in borate buffer) was conducted in aqueous solution whose pH was finally adjusted to 6.2, where the surface charge of both QD800(COOH) (pK_a of carboxyl group = 4.5) and γ-PGA/$MnFe_2O_4$/PLL(PEG) nanogels (as shown in Table 1) remains strong enough to lead facile self-assembly through electrostatic interaction without any particle agglomeration. Figure 2a shows the size and surface morphologies of the synthesized magneto-fluorescent γ-PGA/$MnFe_2O_4$/PLL(PEG)/QD800(COOH) polyelectrolyte nanocomposites (hereafter, MagFL-PEN) characterized by SEM and TEM (inset) after the assembly of QDs. The measured SEM and TEM images implied that the satellites of $MnFe_2O_4$ nanoparticles were encapsulated inside MagFL-PEN, while NIR emitting QD800(COOH) were coated on the surface MagFL-PEN. The presence of $MnFe_2O_4$ and QD800(COOH) in the fabricated MagFL-PEN was also verified by energy-dispersive X-ray analysis (EDX), as shown in Figure 2b, indicating that both $MnFe_2O_4$ and QD800(COOH) were loaded in MagFL-PEN. We have investigated the magnetic and NIR fluorescent properties of the fabricated MagFL-PEN as high-performance MR/NIR dual-modality imaging nanoprobes. The high-resolution MR T_2 relaxation efficiency of the synthesized contrast agents of MagFL-PEN was determined by measuring transverse relaxivity (r_2) at 200 MHz on an MRI scanner. The relaxivity (r_2) of MagFL-PEN represents the reciprocal of the T_2 relaxation time per unit concentration of metal ions, with unit of (Fe + Mn) mM^{-1} s^{-1}. Figure 2c shows that the measured r_2 value of the MagFL-PEN was 436.8 (Fe + Mn) mM^{-1} s^{-1}, more than 2.3-fold higher than those of conventional SPIO contrast agents (120 and 189 mM^{-1} s^{-1} for Feridex and Resovist, respectively). It is assumed that this significant increase in the r_2 value arises from the synergic magnetism of multicore $MnFe_2O_4$ nanoparticle satellites encapsulated in the MagFL-PEN matrix. Moreover, this value is also higher than that of other previous reports, for example, single $MnFe_2O_4$ nanoparticles coated with lipid micelle (66 (Fe + Mn) mM^{-1} s^{-1})[50] and $MnFe_2O_4$ cluster loaded

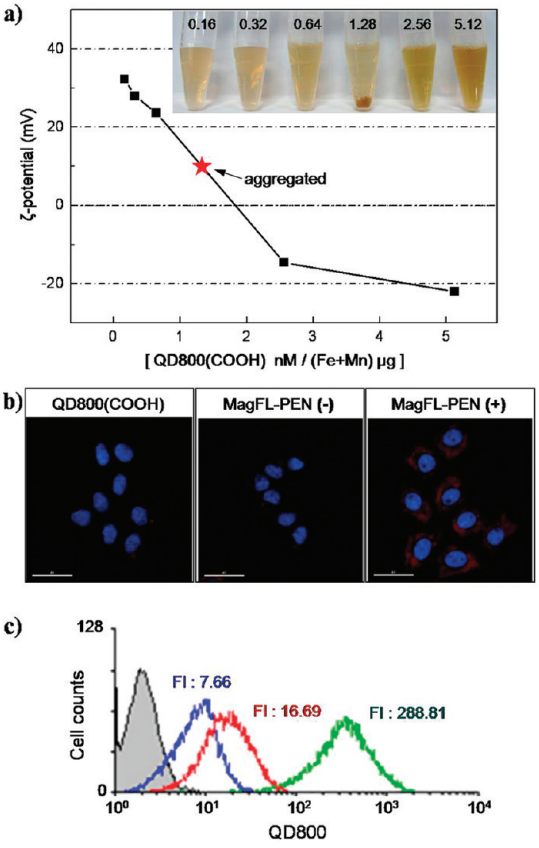

Figure 3. (a) ζ-Potential change and particle stability of MagFL-PEN solution at different concentration ratio between QD800(COOH) and (Fe + Mn). (b) Fluorescence images of HeLa cells treated with QD800(COOH), negatively charged MagFL-PEN, and positively charged MagFL-PEN. (c) FACS analysis of HeLa cells treated with QD800(COOH) (blue), negatively charged MagFL-PEN (red), and positively charged MagFL-PEN (green). Scale bars in (b), 40 μm.

amphiphilic polymer micelle (270 (Fe + Mn) mM^{-1} s^{-1}).[50] In addition to the excellent T_2-darkening effect, the MagFL-PEN also generated a strong NIR fluorescence signal (λ_{ex} = 488 nm) (Figure 2d). When NIR light was illuminated on MagFL-PEN solutions, strong NIR fluorescence signals and images were obtained, while there was no NIR signal from the control samples (γ-PGA/$MnFe_2O_4$/PLL(PEG)).

We have adjusted the amount of adsorbed QD800-(COOH) to keep the net surface charge of MagFL-PEN positive, resulting in efficient intracellular delivery. The influence of the surface decoration of γ-PGA/$MnFe_2O_4$/PLL(PEG) with QD800(COOH) on the relative stability/aggregation behavior was measured analyzed by DLS (Table 2 and Figure 3a). The ζ-potential change and particle stability of MagFL-PEN solution at different concentration ratio between QD800(COOH) and (Fe + Mn) is shown in Figure 3a. When the concentration of QD800(COOH) per (Fe + Mn) contents in the solution was increased up to 0.64 nM/(Fe + Mn) μg, the ζ-potential showed positive value (+23.62 mV), while the ζ-potential value changed into a negative value (−14.53 mV) when the concentration reached

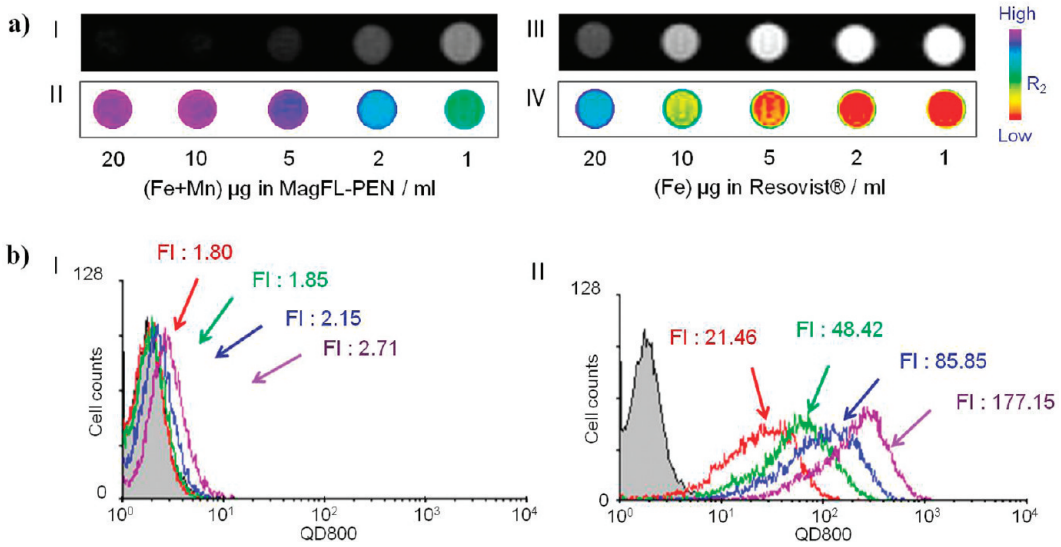

Figure 4. High-performance MR/NIR dual-modality imaging properties of MagFL-PEN. (a) T_2-weighted MR images of HeLa cells treated with MagFL-PEN (I,II) and Resovist (III,IV) (I, III in white/black and II,IV in pseudo color). (b) FACS analysis of HeLa cells labeled with various concentrations of QD800(COOH) and MagFL-PEN (I, QD800(COOH); II, MagFL-PEN) at 12.5 (red), 25 (green), 50 (blue), and 100 pM (purple).

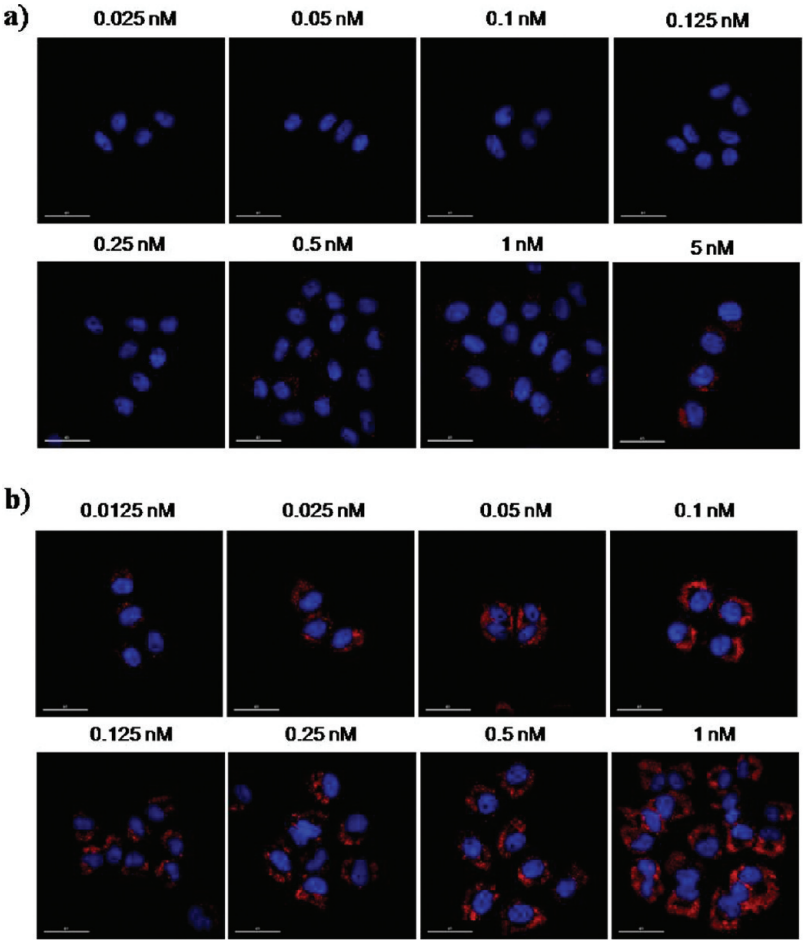

Figure 5. Fluorescence microscope images of HeLa cells labeled with (a) QD800(COOH) and (b) MagFL-PEN at various concentration of QD800(COOH). Scale bars, 40 μm.

2.56 nM/(Fe + Mn) μg (Figure 3a). Moreover, we have investigated the intracellular delivery efficiency of MagFL-PEN, whose net surface charges are negative and positive, respectively (Figure 3b,c). The intracellular

delivery efficiency of MagFL-PEN(+) was about 17 times higher than that of MagFL-PEN(−), indicating that the positive surface charge is one of the possible factors that can explain the high intracellular delivery capacity of MagFL-PEN (Figure 3c). It should be noted that the MagFL-PEN was unstable and precipitated as shown in Figure 3a when the concentration of QD800-(COOH) per (Fe + Mn) contents was in the intermediate region between 0.64 and 2.56 (for an example of 1.28). So, the relative concentration of QD800(COOH) to (Fe + Mn) in MagFL-PEN should be carefully controlled, considering the stability and intracellular delivery capacity of multimodal imaging nanoprobe.

To demonstrate the application of the MagFL-PEN as a highly sensitive MR/NIR multimodal cellular imaging nanoprobe, we investigated the cell labeling efficiency of them using a human cancer cell line. Figure 4a,b shows the high-performance capability of the MagFL-PEN in HeLa cell labeling. Concerning MR performance, the cell labeling efficiency of MagFL-PEN was compared with that of the commercialized MR contrast agent, Resovist. In order to ensure treatment of the same condition of Fe (and Mn) between MagFL-PEN and Resovist, the aliquot of MagFL-PEN was determined by an inductively coupled plasma atomic emission spectrometer (ICP-AES) system (data not shown). As shown in Figure 4a, the T_2 shortening effect in the MagFL-PEN-labeled cells (I and II) was more dominant than Resovist-labeled cells (III and IV). Note that the enhancement of negative contrast (*i.e.*, darkening effect) of MagFL-PEN at 2 μg/mL concentration was similar to that of Resovist at 20 μg/mL concentration. Considering that about 100 μg Fe/mL of Resovist is usually used for labeling cells in the clinical fields,[51] the MagFL-PEN, even at a concentration of Fe (and Mn) content diluted by 50 times, can generate the similar MR contrast enhancement compared to Resovist. We also employed flow cytometry to quantify the labeling efficiency of HeLa cells by the MagFL-PEN or the QD800(COOH) themselves. There was no distinct increase in QD800(COOH) emissions over the background in cells treated with QD800(COOH) alone (I in Figure 4b), which is in good agreement with the fluorescence microscopy experiments that also showed poor internalization efficiency at subnanomolar concentrations of the probes (Figure 5a). At a QD800-(COOH) concentration of 1−5 nM, the increase in fluorescence of HeLa cells began to be observed clearly. In contrast, the delivery efficiency of MagFL-PEN to HeLa cells was markedly improved, and the extent of labeling was increased with the concentration of the probes (II in Figure 4b and Figure 5b). The fluorescence microscopy images of the MagFL-PEN-labeled cells even at 12.5 pM, in our experiment condition, were able to be clearly observed. It should be noted that the labeling efficiency of MagFL-PEN was approximately 65-fold higher compared to that of the

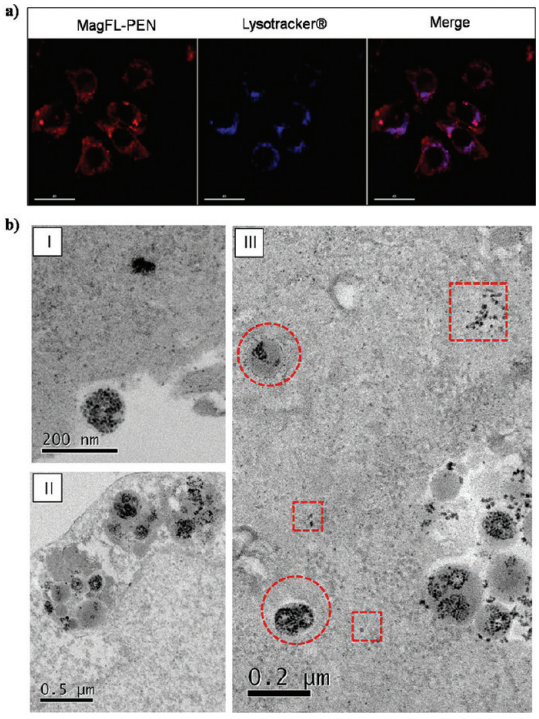

Figure 6. Intracellular delivery of MagFL-PEN. (a) Fluorescence microscope images of HeLa cells treated with MagFL-PEN: MagFL-PEN (red, pseudo color) and Lysotracker (blue). (b) Bio-TEM images of HeLa cells treated with MagFL-PEN (I→II, from outside to early endosome; III, from endosome to lysosome and/or cytosol). Scale bars in (a), 40 μm.

QD800(COOH) only after 3 h incubation time, even at the concentration of the test (100 pM). On the basis of the Lysotracker-labeled images, we could see that a great deal of the MagFL-PEN was delivered into cytosol, while some of the MagFL-PEN was still observed in lysosome (colocalization with Lysotracker (Figure 6a). Bio-TEM images (Figure 6b) of HeLa cells labeled with the MagFL-PEN also supported that MagFL-PEN entered into cells (I→II, from outside to early endosome) and consequently into lysosome and/or cytosol (III, from endosome to lysosome and/or cytosol).

Although we assume that the dramatic increase in the intracellular delivery efficiency of MagFL-PEN may result from the cationic character of MagFL-PEN, the exact mechanism of how the nanoparticles interact with the cell membrane and enter into the cells is a complex issue and will be investigated in the future. In fact, carboxylic-acid-functionalized quantum dots were reported to be internalized into the cytoplasm regime of macrophage RAW cells without entering the nucleus.[52] Up to now, it has been known that non-receptor-mediated endocytosis is observed frequently in HeLa cells and the non-receptor-mediated endocytosis seems to be a general process occurring in various cells upon ingestion of nanoparticles without having surface-grafted agonists, for example, an intake of carboxylic-acid-functionalized nanodiamonds by 293T

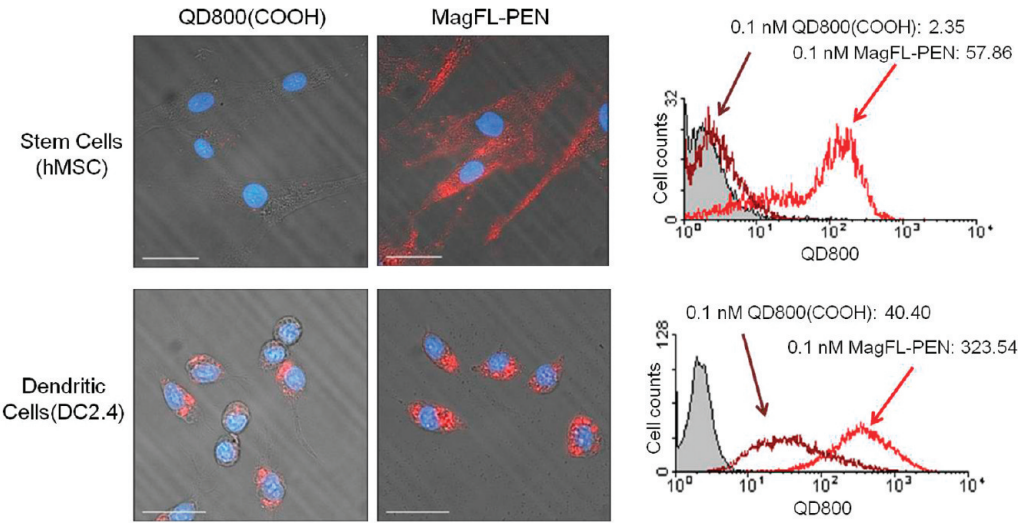

Figure 7. Fluorescence images and FACS analysis of human mesenchymal stem cells (hMSC) and dendritic cells (DC2.4) labeled with QD800(COOH) only and MagFL-PEN. Scale bars, 40 μm.

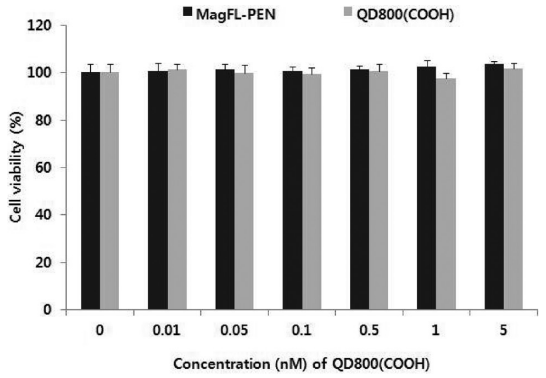

Figure 8. MTT assay of HeLa cells labeled with QD800-(COOH) and MagFL-PEN.

human kidney cells,[53] macrophage RAW cells,[54] human lung A549 epithelial cells, and HFL-1 normal fibroblasts.[55] If we consider the fact that MagFL-PEN was efficiently taken up by HeLa cells, even in the absence of a specific ligand, a non-receptor-mediated endocytosis pathway of HeLa cells may be another factor for the high intracellular delivery efficiency of MagFL-PEN. To demonstrate the potent applications of the MagFL-PEN as a highly sensitive cellular/molecular imaging probe, we have also investigated the cell labeling efficiency of the nanoprobe in other types of phagocytic (dendritic cells) and nonphagocytic cells (stem cells). The experimental data showed that MagFL-PEN could label the stem cells as well as immunotherapeutic cells very efficiently (Figure 7). The positive surface charge of the MagFL-PEN may be one of the factors for the high intracellular delivery efficiency of MagFL-PEN into nonphagocytic stem cells without the use of any cell transfection reagents or mechanical devices.[28,56] Because novel non-invasive multimodal imaging approaches that can combine high sensitivity (as provided by optical imaging techniques) with direct depiction for the high-resolution tracking (as provided by MR imaging) of transplanted stem cells or injected immunotherapeutic dendritic cells in real time are highly required in the clinical trials, the MagFL-PEN can be a tool for labeling and tracking of the therapeutic cells. Regarding the biocompatibility or cytotoxicity of MagFL-PEN, MTT experiments were carried out using HeLa cells to examine the cell viability. As shown in Figure 8, there was little effect of MagFL-PEN on cell viability under the cellular imaging condition used in the fluorescence microscope experiments where the concentration of QDs is up to 0.1 nM in the case of MagFL-PEN.

CONCLUSION

We have developed a facile and robust methodology for the synthesis of novel nanostructured materials for high-performance MR/NIR dual-modality molecular imaging nanoprobes by combining inorganic colloidal chemistry and ionic gelation of biocompatible polyelectrolytes. Due to the high-performance capabilities both in materials properties and in cell labeling efficiency, the polyelectrolyte nanocomposites are expected to be used as highly efficient MR/NIR dual-modality imaging nanoprobe in the detection of cancer cells and monitoring of therapeutic cells *in vivo*. Our findings in this communication are significant for the following reasons. First, this study provides an easy but robust method for the fabrication of multifunctional organic/inorganic hybrid materials using biocompatible polyelectrolyte materials. The polyelectrolyte materials can be used for the convenient phase transfer of magnetic nanoparticles (and/or semiconductor nanocrystals) dispersed in organic solvents into aqueous solutions and provides numerous functional moieties (such as carboxyl, amine), which facilitates further conjugation with biomolecules. Second, it should also be noted that considerably lower concentration of polyelectrolyte

nanocomposites was enough for the labeling and detection of cancer cells. Although the external magnetic field has been widely used to enhance the intracellular delivery efficiency of magnetic nanoparticles into cells, the lower concentrations of polyelectrolyte nanocomposites revealed in this study can be easily used for the labeling of cells without any external magnetic force, due to their higher intracellular delivery capacity.[57] This should be emphasized because we can minimize the possible toxicity effect of the nanoprobe on cell viability and their biological function by reducing the concentration. Third, the NIR fluorescence imaging modality of MR/NIR dual-modality imaging nanoprobe can be applied for *in vivo* imaging fields, where real-time guidance is very important.[21−24] For an example, high-performance MR/NIR dual-modality imaging nanoprobe has great potential for future clinical imaging fields such as disease diagnosis at a preoperative stage (with MRI), surgical guidance at an operative stage (with NIR), and finally pathological analysis at a postoperative stage (with NIR) due to their multiple imaging modalities.[58] Fourth, the polyelectrolyte gel nanocomposites can be used as a theranostic platform technology by incorporating various kinds of therapeutic molecules, such as chemical drugs, DNA, siRNA, proteins, and therapeutic cells.[59−61]

MATERIALS AND METHODS

Synthesis of MagFL-PEN. Eight nanometers of manganese-doped superparamagnetic iron oxide nanoparticles ($MnFe_2O_4$) was first prepared by the thermal decomposition method, as detailed in the literature.[62] $MnFe_2O_4$ nanoparticles in hexane (10 mg/mL) were precipitated with excess methanol in order to wash out remaining surfactants such as oleic acid and oleylamine. After centrifugation, the supernatant was completely removed and the precipitation was redispersed in chloroform. Then, we modified the surface of $MnFe_2O_4$ nanoparticles *via* γ-PGA (poly(γ-glutamic acid), 500 kDa, Bioleaders Coporation, Republic of Korea) to transfer the nanoparticles from hexane into aqueous phase. Ten milliliters of $MnFe_2O_4$ solution in chloroform was mixed with γ-PGA dissolved in DMSO (10 mg/mL) at a 1:1 mass ratio. The mixture was stirred at 60 °C for 2 h under nitrogen gas flow. After cooling to room temperature, the γ-PGA-coated $MnFe_2O_4$ nanoparticles were washed with a cosolvent of ethanol, chloroform, and hexane (1:1:2) to remove unreacted compounds and precipitated by the centrifuge at 5000 rpm for 10 min. The supernatant was completely removed, and then the black pellets of γ-PGA-coated $MnFe_2O_4$ nanoparticles were redispersed in 20 mL of $NaHCO_3$ solution (50 mM, pH 8.5) by ultratip sonication (VCX 750, Sonics & Materials, USA) for 4 min. Finally, the solution was filtered through a 0.22 μm syringe filter. For fabrication of γ-PGA/$MnFe_2O_4$/PLL(PEG) complex *via* ionic assembly between PLL (poly-L-lysine, 15−30 kDa, Sigma-Aldrich, USA) and γ-PGA-coated $MnFe_2O_4$ nanoparticles, 1 mL of γ-PGA-coated $MnFe_2O_4$ nanoparticle solutions was added to the solution dissolved 18 mg of PLL in 10 mL of distilled water with vigorously stirring for 2 h. To increase the stability of ionic nanocomplex at various pH and salt (NaCl) concentrations, 1 mg/mL of 1-ethyl-3-(3-dimethylaminopropyl)carbodiimide hydrochloride (EDC.HCl) (Sigma-Aldrich, USA) could be added. For the PEGylated surface of γ-PGA/$MnFe_2O_4$/PLL, 250 mg of mPEG-NHS (methoxy poly(ethylene glycol)succinimidyl glutarate, 5 kDa, SunBio, Inc., Republic of Korea) was mixed with 10 mL of γ-PGA/$MnFe_2O_4$/PLL solution and reacted for 12 h. The final solution was washed with distilled water by centrifugation (6000 rpm, 10 min) two times to remove unreacted compounds and was redispersed in 10 mL of distilled water. The γ-PGA/$MnFe_2O_4$/PLL(PEG) solution was stored at 4 °C for later use. Various concentrations of carboxylated quantum dot nanocrystals (QD800(COOH): Qdot800 ITK, 8 μM, Invitrogen, USA) were mixed with γ-PGA/$MnFe_2O_4$/PLL(PEG) solution (50 (Fe + Mn) μg/mL) in dark field. After centrifugation, the magnetofluorescent γ-PGA/$MnFe_2O_4$/PLL(PEG)/QD800(COOH) polyelectrolyte nanocomposites (hereafter, MagFL-PEN) solutions were stored at 4 °C in dark field.

Characterization of γ-PGA/$MnFe_2O_4$/PLL(PEG) and MagFL-PEN. The surface modification of γ-PGA/$MnFe_2O_4$ was examined by FTIR-ATR (ALPHA-P, Bruker Optic, Germany) after freeze-drying. Hydrodynamic particle diameter and ζ-potential were measured by a DLS spectrometer (ELS-Z, Otsuka Electronics, Japan). Morphology and structure of γ-PGA/$MnFe_2O_4$/PLL(PEG) nanoparticles were determined using FE-TEM (JEM-2100F HR, JEOL Ltd., Japan) and FE-SEM (JSM-7000F, JEOL Ltd., Japan). For TEM imaging and energy-dispersive X-ray analysis (EDX), γ-PGA/$MnFe_2O_4$/PLL(PEG) and MagFL-PEN solution were dropped on the Formvar/carbon-coated copper grids and the residual solution was removed using filter paper. This process was repeated three times, and the grid was dried under vacuum. SEM images were obtained after γ-PGA/$MnFe_2O_4$/PLL(PEG) and MagFL-PEN solution was freeze-dried. T_2-weighted images and T_2 relaxation time of γ-PGA-coated $MnFe_2O_4$ and MagFL-PEN were acquired using a Bruker Biospin 4.7 T scanner (Bruker BioSpin, Germany) with a quadrature birdcage RF coil (35 mm inner diameter, Bruker). The content of metal ions (Fe, Mn) in MagFL-PEN was measured by an inductively coupled plasma atomic emission spectrophotometer (ICP-AES, Optima 4300DV, Perkin-Elmer, MA, USA). The T_2-weighted images were acquired with a conventional spin echo acquisition (TR = 5000 ms) with TE values ranging from 6 to 170 ms. Relaxivity value of r_2 was calculated through the curve fitting of T_2-measured relaxation rates ($R_2 = 1/T_2$, s^{-1}) *versus* the magnetic atom [Fe + Mn] concentration (mM). Fluorescence properties of MagFL-PEN (λ_{ex} = 488 nm) were carried out using fluorescence spectrometer (LS 55 Luminescence Spectrometer, Perkin-Elmer, USA)

Cell Culture and Imaging. HeLa, a human cervical cancer cell line, was obtained from the ATCC (Manassas, VA, USA). Cells were cultured in Dulbecco's modified Eagle's medium (DMEM, Gibco-BRL, Grand Island, NY, USA) supplemented with 2 mM glutamine, 10% (v/v) heat-inactivated fetal bovine serum (FBS; Gibco, USA), 50 IU/mL penicillin, and 50 μg/mL streptomycin (Gibco) at 37 °C in humidified air containing 5% CO_2. DC2.4 cells, which were previously characterized as an immature murine DC line (H-2b) (32), were obtained from Dr. Kenneth L. Rock (Dana-Farber Cancer Institute, Boston, MA, USA) and cultured in DMEM supplemented with 10% heat-inactivated FBS, 50 IU/mL penicillin, and 50 μg/mL streptomycin. Human mesenchymal stem cells (hMSC) were cultured in MSCGM (basal medium (MSCBM) supplemented with MSCGM SingleQuot Kit, Lonza). To visualize the intracellular delivery of MagFL-PEN, various concentrations of MagFL-PEN were treated with HeLa cells and the fluorescence images of them were obtained as a function of time. For these experiments, HeLa cells were plated in a μ-slide 8-well microscopy chamber at a density of 3×10^3 cells in culture medium. Cells were allowed to seed for 24 h and then incubated with MagFL-PEN (1 nM) at 37 °C for 24 h in culture medium. Unbounded MagFL-PEN was removed by washing with phosphate buffered saline (PBS, Gibco). Cells were fixed with cytofix/cytoperm solution (BD PharMingen, San Diego, CA, USA) for 10 min and blocked for 30 min in PBS containing 1% bovine serum albumin (BSA; Sigma, St Louis, MO, USA). To detect intracellular localization of QD800(COOH) to lysosomes, cells were

stained with the lysosomal marker, Lysotracker Blue DND-22 (Invitrogen, Molecular Probes), for 30 min. Fluorescence images were obtained by using a Deltavision RT (Applied Precision Technologies, Issaquah, WA, USA).

Flow Cytometry. HeLa cells were seed on 6-well plates at a density of 1×10^5 cells/well in the culture medium. Various concentrations of MagFL-PEN and QD800(COOH) nanoparticles were added to each well and incubated for 24 h. After washing with PBS, the cells were analyzed by using a FACScalibur (Becton Dickinson, Mountain View, CA, USA). More than 10 000 events were collected. The data were analyzed using a WinMDI 2.9 (Joseph Trotter, Scripps Institute, La Jolla, CA, USA) by gating on the live cell populations.

Cytotoxicity. The cytotoxicity effects of MagFL-PEN and QD800(COOH) nanoparticles were evaluated by using a standard 3-(4,5-dimethylthiazol-2-yl)-2,5-diphenyltetrazolium bromide (MTT, sigma) assay. Briefly, cells were seed on 96-well plates at a density of 5×10^3 cells/well in the culture medium. Various concentrations of MagFL-PEN and QD800(COOH) nanoparticles in 100 μL culture medium were added to each well and incubated for 24 h. Subsequently, the cells were replaced in 100 μL culture medium containing 0.5 mg/mL MTT reagent and incubated for an additional 2 h. Finally, the absorbance at 570 nm was measured using a VICTOR3 microplate reader (PerkinElmer, Waltham, MA, USA).

Acknowledgment. The authors acknowledge the financial supports from the National Research Foundation of Korea (NRF) grant funded by the Korea government (MEST) (No. 2010-0026793), the National Research Facilities & Equipment Centre grant, the National Agenda Project grant from Korea Research Council of Fundamental Science and Technology, the grant from Korea Basic Science Institute (T31403), and the National Research Foundation of Korea Grant funded by the Korean Government (MEST) (2009, University-Institute cooperation program).

REFERENCES AND NOTES

1. Barreto, J. A.; O'Malley, W.; Kubeil, M.; Graham, B.; Stephan, H.; Spiccia, L. Nanomaterials: Applications in Cancer Imaging and Therapy. *Adv. Mater.* **2011**, *23*, H18–H40.
2. Cherry, S. R. Multimodality *In Vivo* Imaging Systems: Twice the Power or Double the Trouble? *Annu. Rev. Biomed. Eng.* **2006**, *8*, 35–62.
3. Lee, J. E.; Lee, N.; Kim, H.; Kim, J.; Choi, S. H.; Kim, J. H.; Kim, T.; Song, I. C.; Park, S. P.; Moon, W. K.; *et al.* Uniform Mesoporous Dye-Doped Silica Nanoparticles Decorated with Multiple Magnetite Nanocrystals for Simultaneous Enhanced Magnetic Resonance Imaging, Fluorescence Imaging, and Drug Delivery. *J. Am. Chem. Soc.* **2010**, *132*, 552–557.
4. Mulder, W. J. M.; Strijkers, G. J.; Van Tilborg, G. A. F.; Cormode, D. P.; Fayad, Z. A.; Nicolay, K. Nanoparticulate Assemblies of Amphiphiles and Diagnostically Active Materials for Multimodality Imaging. *Acc. Chem. Res.* **2009**, *42*, 904–914.
5. Roth, B. J. The Role of Magnetic Forces in Biology and Medicine. *Exp. Biol. Med.* **2011**, *236*, 132–137.
6. Huh, Y. M.; Jun, Y. W.; Song, H. T.; Kim, S.; Choi, J. S.; Lee, J. H.; Yoon, S.; Kim, K. S.; Shin, J. S.; Suh, J. S.; *et al. In Vivo* Magnetic Resonance Detection of Cancer by Using Multifunctional Magnetic Nanocrystals. *J. Am. Chem. Soc.* **2005**, *127*, 12387–12391.
7. Lee, H.; Yu, M. K.; Park, S.; Moon, S.; Min, J. J.; Jeong, Y. Y.; Kang, H. W.; Jon, S. Thermally Cross-Linked Superparamagnetic Iron Oxide Nanoparticles: Synthesis and Application as a Dual Imaging Probe for Cancer *in Vivo*. *J. Am. Chem. Soc.* **2007**, *129*, 12739–12745.
8. Santra, S.; Bagwe, R. P.; Dutta, D.; Stanley, J. T.; Walter, G. A.; Tan, W.; Moudgil, B. M.; Mericle, R. A. Synthesis and Characterization of Fluorescent, Radio-Opaque, and Paramagnetic Silica Nanoparticles for Multimodal Bioimaging Applications. *Adv. Mater.* **2005**, *17*, 2165–2169.
9. Bhushan, K. R.; Misra, P.; Liu, F.; Mathur, S.; Lenkinski, R. E.; Frangioni, J. V. Detection of Breast Cancer Microcalcifications Using a Dual-Modality SPECT/NIR Fluorescent Probe. *J. Am. Chem. Soc.* **2008**, *130*, 17648.
10. Erogbogbo, F.; Yong, K. T.; Hu, R.; Law, W. C.; Ding, H.; Chang, C. W.; Prasad, P. N.; Swihart, M. T. Biocompatible Magnetofluorescent Probes: Luminescent Silicon Quantum Dots Coupled with Superparamagnetic Iron(III) Oxide. *ACS Nano* **2010**, *4*, 5131–5138.
11. Sun, C. R.; Du, K.; Fang, C.; Bhattarai, N.; Veiseh, O.; Kievit, F.; Stephen, Z.; Lee, D. H.; Ellenbogen, R. G.; Ratner, B.; *et al.* PEG-Mediated Synthesis of Highly Dispersive Multifunctional Superparamagnetic Nanoparticles: Their Physicochemical Properties and Function *in Vivo*. *ACS Nano* **2010**, *4*, 2402–2410.
12. Lim, Y. T.; Noh, Y. W.; Cho, J. H.; Han, J. H.; Choi, B. S.; Kwon, J.; Hong, K. S.; Gokarna, A.; Cho, Y. H.; Chung, B. H. Multiplexed Imaging of Therapeutic Cells with Multispectrally Encoded Magnetofluorescent Nanocomposite Emulsions. *J. Am. Chem. Soc.* **2009**, *131*, 17145–17154.
13. Ali, Z.; Abbasi, A. Z.; Zhang, F.; Arosio, P.; Lascialfari, A.; Casula, M. F.; Wenk, A.; Kreyling, W.; Plapper, R.; Seidel, M.; *et al.* Multifunctional Nanoparticles for Dual Imaging. *Anal. Chem.* **2011**, *83*, 2877–2882.
14. Frullano, L.; Catana, C.; Benner, T.; Sherry, A. D.; Caravan, P. Bimodal MR-PET Agent for Quantitative pH Imaging. *Angew. Chem., Int. Ed.* **2010**, *49*, 2382–2384.
15. Choi, J. S.; Park, J. C.; Nah, H.; Woo, S.; Oh, J.; Kim, K. M.; Cheon, G. J.; Chang, Y.; Yoo, J.; Cheon, J. A Hybrid Nanoparticle Probe for Dual-Modality Positron Emission Tomography and Magnetic Resonance Imaging. *Angew. Chem., Int. Ed.* **2008**, *47*, 6259–6262.
16. Jadvar, H.; Connolly, L. P.; Fahey, F. H.; Shulkin, B. L. PET and PET/CT in Pediatric Oncology. *Semin. Nucl. Med.* **2007**, *37*, 316–331.
17. Kwee, T. C.; Basu, S.; Cheng, G.; Alavi, A. FDG PET/CT in Carcinoma of Unknown Primary. *Eur. J. Nucl. Med. Mol. Imaging* **2010**, *37*, 635–644.
18. Pittet, M. J.; Swirski, F. K.; Reynolds, F.; Josephson, L.; Weissleder, R. Labeling of Immune Cells for *In Vivo* Imaging Using Magnetofluorescent Nanoparticles. *Nat. Protoc.* **2006**, *1*, 73–79.
19. Lim, Y. T.; Kim, J. K.; Noh, Y. W.; Cho, M. Y.; Chung, B. H. Multifunctional Silica Nanocapsule with a Single Surface Hole. *Small* **2009**, *5*, 324–328.
20. Lim, Y. T.; Noh, Y. W.; Han, J. H.; Cai, Q. Y.; Yoon, K. H.; Chung, B. H. Biocompatible Polymer-Nanoparticle-Based Bimodal Imaging Contrast Agents for the Labeling and Tracking of Dendritic Cells. *Small* **2008**, *4*, 1640–1645.
21. Kim, S.; Lim, Y. T.; Soltesz, E. G.; De Grand, A. M.; Lee, J.; Nakayama, A.; Parker, J. A.; Mihaljevic, T.; Laurence, R. G.; Dor, D. M.; *et al.* Near-Infrared Fluorescent Type II Quantum Dots for Sentinel Lymph Node Mapping. *Nat. Biotechnol.* **2004**, *22*, 93–97.
22. Choi, H. S.; Ipe, B. I.; Misra, P.; Lee, J. H.; Bawendi, M. G.; Frangioni, J. V. Tissue- and Organ-Selective Biodistribution of NIR Fluorescent Quantum Dots. *Nano Lett.* **2009**, *9*, 2354–2359.
23. Frangioni, J. V. *In Vivo* Near-Infrared Fluorescence Imaging. *Curr. Opin. Chem. Biol.* **2003**, *7*, 626–634.
24. Noh, Y. W.; Lim, Y. T.; Chung, B. H. Noninvasive Imaging of Dendritic Cell Migration into Lymph Nodes Using Near-Infrared Fluorescent Semiconductor Nanocrystals. *FASEB J.* **2008**, *22*, 3908–3918.
25. Lee, N.; Kim, H.; Choi, S. H.; Park, M.; Kim, D.; Kim, H. C.; Choi, Y.; Lin, S.; Kim, B. H.; Jung, H. S.; *et al.* Magnetosome-like Ferrimagnetic Iron Oxide Nanocubes for Highly Sensitive MRI of Single Cells and Transplanted Pancreatic Islets. *Proc. Natl. Acad. Sci. U.S.A.* **2011**, *108*, 2662–2667.
26. Shapiro, E. M.; Skrtic, S.; Sharer, K.; Hill, J. M.; Dunbar, C. E.; Koretsky, A. P. MRI Detection of Single Particles for Cellular Imaging. *Proc. Natl. Acad. Sci. U.S.A.* **2004**, *101*, 10901–10906.
27. Jarzyna, P. A.; Skajaa, T.; Gianella, A.; Cormode, D. P.; Samber, D. D.; Dickson, S. D.; Chen, W.; Griffioen, A. W.; Fayad, Z. A.; Mulder, W. J. M. Iron Oxide Core Oil-in-Water Emulsions as a Multifunctional Nanoparticle Platform for

Tumor Targeting and Imaging. *Biomaterials* **2009**, *30*, 6947–6954.
28. Thorek, D. L. J.; Tsourkas, A. Size, Charge and Concentration Dependent Uptake of Iron Oxide Particles by Non-phagocytic Cells. *Biomaterials* **2008**, *29*, 3583–3590.
29. Lee, J. H.; Huh, Y. M.; Jun, Y.; Seo, J.; Jang, J.; Song, H. T.; Kim, S.; Cho, E. J.; Yoon, H. G.; Suh, J. S.; *et al.* Artificially Engineered Magnetic Nanoparticles for Ultra-sensitive Molecular Imaging. *Nat. Med.* **2007**, *13*, 95–99.
30. Vestal, C. R.; Zhang, Z. J. Synthesis and Magnetic Characterization of Mn and Co Spinel Ferrite-Silica Nanoparticles with Tunable Magnetic Core. *Nano Lett.* **2003**, *3*, 1739–1743.
31. Masala, O.; Seshadri, R. Magnetic Properties of Capped, Soluble $MnFe_2O_4$ Nanoparticles. *Chem. Phys. Lett.* **2005**, *402*, 160–164.
32. Yoon, T. J.; Lee, H.; Shao, H. L.; Weissleder, R. Highly Magnetic Core−Shell Nanoparticles with a Unique Magnetization Mechanism. *Angew. Chem., Int. Ed.* **2011**, *50*, 4663–4666.
33. Sun, B.; Sun, M. J.; Gu, Z.; Shen, Q. D.; Jiang, S. J.; Xu, Y.; Wang, Y. Conjugated Polymer Fluorescence Probe for Intracellular Imaging of Magnetic Nanoparticles. *Macromolecules* **2010**, *43*, 10348–10354.
34. Thompson, C.; Cheng, W. P.; Gadad, P.; Skene, K.; Smith, M.; Smith, G.; McKinnon, A.; Knott, R. Uptake and Transport of Novel Amphiphilic Polyelectrolyte-Insulin Nanocomplexes by Caco-2 Cells—Towards Oral Insulin. *Pharm. Res.* **2011**, *28*, 886–896.
35. Schneider, G. F.; Subr, V.; Ulbrich, K.; Decher, G. Multifunctional Cytotoxic Stealth Nanoparticles. A Model Approach with Potential for Cancer Therapy. *Nano Lett.* **2009**, *9*, 636–642.
36. Kim, T. W.; Lee, T. Y.; Bae, F. C.; Hahm, J. H.; Kim, Y. H.; Park, C.; Kang, T. H.; Kim, C. J.; Sung, M. H.; Poo, H. Oral Administration of High Molecular Mass Poly-γ-Glutamate Induces NK Cell-Mediated Antitumor Immunity. *J. Immunol.* **2007**, *179*, 775–780.
37. Bae, S. R.; Park, C.; Choi, J. C.; Poo, H.; Kim, C. J.; Sung, M. H. Effects of Ultra High Molecular Weight Poly-γ-Glutamic Acid from *Bacillus subtilis* (Chungkookjang) on Corneal Wound Healing. *J. Microbiol. Biotechnol.* **2010**, *20*, 803–808.
38. Okamoto, S.; Matsuura, M.; Akagi, T.; Akashi, M.; Tanimoto, T.; Ishikawa, T.; Takahashi, M.; Yamanishi, K.; Mori, Y. Poly(γ-glutamic acid) Nano-particles Combined with Mucosal Influenza Virus Hemagglutinin Vaccine Protects Against Influenza Virus Infection in Mice. *Vaccine* **2009**, *27*, 5896–5905.
39. Manocha, B.; Margaritis, A. Production and Characterization of γ-Polyglutarnic Acid Nanoparticles for Controlled Anticancer Drug Release. *Crit. Rev. Biotechnol.* **2008**, *28*, 83–99.
40. Shih, I. L.; Van, Y. T.; Shen, M. H. Biomedical Applications of Chemically and Microbiologically Synthesized Poly-(glutamic acid) and Poly(lysine). *Mini-Rev. Med. Chem.* **2004**, *4*, 179–188.
41. Park, T. G.; Jeong, J. H.; Kim, S. W. Current Status of Polymeric Gene Delivery Systems. *Adv. Drug Delivery Rev.* **2006**, *58*, 467–486.
42. Malmsten, M.; Bysell, H.; Hansson, P. Biomacromolecules in Microgels—Opportunities and Challenges for Drug Delivery. *Curr. Opin. Colloid Interface Sci.* **2010**, *15*, 435–444.
43. Zhang, L.; He, R.; Gu, H. C. Oleic Acid Coating on the Monodisperse Magnetite Nanoparticles. *Appl. Surf. Sci.* **2006**, *253*, 2611–2617.
44. Huang, G.; Zhang, C. F.; Li, S. Z.; Khemtong, C.; Yang, S. G.; Tian, R. H.; Minna, J. D.; Brown, K. C.; Gao, J. M. A Novel Strategy for Surface Modification of Superparamagnetic Iron Oxide Nanoparticles for Lung Cancer Imaging. *J. Mater. Chem.* **2009**, *19*, 6367–6372.
45. Yang, J.; Lee, J. Y.; Ying, J. Y. Phase Transfer and Its Applications in Nanotechnology. *Chem. Soc. Rev.* **2011**, *40*, 1672–1696.
46. Pellegrino, T.; Manna, L.; Kudera, S.; Liedl, T.; Koktysh, D.; Rogach, A. L.; Keller, S.; Radler, J.; Natile, G.; Parak, W. J. Hydrophobic Nanocrystals Coated with an Amphiphilic Polymer Shell: A General Route to Water Soluble Nanocrystals. *Nano Lett.* **2004**, *4*, 703–707.
47. Stewart, M. H.; Susumu, K.; Mei, B. C.; Medintz, I. L.; Delehanty, J. B.; Blanco-Canosa, J. B.; Dawson, P. E.; Mattoussi, H. Multidentate Poly(ethylene glycol) Ligands Provide Colloidal Stability to Semiconductor and Metallic Nanocrystals in Extreme Conditions. *J. Am. Chem. Soc.* **2010**, *132*, 9804–9813.
48. Kim, B. S.; Qiu, J. M.; Wang, J. P.; Taton, T. A. Magnetomicelles: Composite Nanostructures from Magnetic Nanoparticles and Cross-Linked Amphiphilic Block Copolymers. *Nano Lett.* **2005**, *5*, 1987–1991.
49. Li, H.; Shih, W. Y.; Shih, W. H. Non-Heavy-Metal ZnS Quantum Dots with Bright Blue Photoluminescence by a One-Step Aqueous Synthesis. *Nanotechnology* **2007**, *18*, 205604.
50. Lu, J.; Ma, S. L.; Sun, J. Y.; Xia, C. C.; Liu, C.; Wang, Z. Y.; Zhao, X. N.; Gao, F. B.; Gong, Q. Y.; Song, B.; *et al.* Manganese Ferrite Nanoparticle Micellar Nanocomposites as MRI Contrast Agent for Liver Imaging. *Biomaterials* **2009**, *30*, 2919–2928.
51. Toso, C.; Valle, J. P.; Morel, P.; Ris, F.; Demuylder-Mischler, S.; Lepetit-Coiffe, M.; Marangon, N.; Saudek, F.; Shapiro, A. M. J.; Bosco, D.; *et al.* Clinical Magnetic Resonance Imaging of Pancreatic Islet Grafts after Iron Nanoparticle Labeling. *Am. J. Transplant.* **2008**, *8*, 701–706.
52. Ushizawa, K.; Sato, Y.; Mitsumori, T.; Machinami, T.; Ueda, T.; Ando, T. Covalent Immobilization of DNA on Diamond and Its Verification by Diffuse Reflectance Infrared Spectroscopy. *Chem. Phys. Lett.* **2002**, *351*, 105–108.
53. Gruber, A.; Drabenstedt, A.; Tietz, C.; Fleury, L.; Wrachtrup, J.; von Borczyskowski, C. Scanning Confocal Optical Microscopy and Magnetic Resonance on Single Defect Centers. *Science* **1997**, *276*, 2012–2014.
54. Huang, H.; Pierstorff, E.; Osawa, E.; Ho, D. Active Nanodiamond Hydrogels for Chemotherapeutic Delivery. *Nano Lett.* **2007**, *7*, 3305–3314.
55. Liu, K. K.; Cheng, C. L.; Chang, C. C.; Chao, J. I. Biocompatible and Detectable Carboxylated Nanodiamond on Human Cell. *Nanotechnology* **2007**, *18*, 325102.
56. Soenen, S. J. H.; Illyes, E.; Vercauteren, D.; Braeckmans, K.; Majer, Z.; De Smedt, S. C.; De Cuyper, M. The Role of Nanoparticle Concentration-Dependent Induction of Cellular Stress in the Internalization of Non-toxic Cationic Magnetoliposomes. *Biomaterials* **2009**, *30*, 6803–6813.
57. Kamei, K.; Mukai, Y.; Kojima, H.; Yoshikawa, T.; Yoshikawa, M.; Kiyohara, G.; Yamamoto, T. A.; Yoshioka, Y.; Okada, N.; Seino, S.; *et al.* Direct Cell Entry of Gold/Iron-Oxide Magnetic Nanoparticles in Adenovirus Mediated Gene Delivery. *Biomaterials* **2009**, *30*, 1809–1814.
58. Kircher, M. F.; Mahmood, U.; King, R. S.; Weissleder, R.; Josephson, L. A Multimodal Nanoparticle for Preoperative Magnetic Resonance Imaging and Intraoperative Optical Brain Tumor Delineation. *Cancer Res.* **2003**, *63*, 8122–8125.
59. Yu, M. K.; Jeong, Y. Y.; Park, J.; Park, S.; Kim, J. W.; Min, J. J.; Kim, K.; Jon, S. Drug-Loaded Superparamagnetic Iron Oxide Nanoparticles for Combined Cancer Imaging and Therapy *in Vivo*. *Angew. Chem., Int. Ed.* **2008**, *47*, 5362–5365.
60. Kim, J.; Kim, H. S.; Lee, N.; Kim, T.; Kim, H.; Yu, T.; Song, I. C.; Moon, W. K.; Hyeon, T. Multifunctional Uniform Nanoparticles Composed of a Magnetite Nanocrystal Core and a Mesoporous Silica Shell for Magnetic Resonance and Fluorescence Imaging and for Drug Delivery. *Angew. Chem., Int. Ed.* **2008**, *47*, 8438–8441.
61. Yang, J.; Lee, C. H.; Ko, H. J.; Suh, J. S.; Yoon, H. G.; Lee, K.; Huh, Y. M.; Haam, S. Multifunctional Magneto-Polymeric Nanohybrids for Targeted Detection and Synergistic Therapeutic Effects on Breast Cancer. *Angew. Chem., Int. Ed.* **2007**, *46*, 8836–8839.
62. Lee, H.; Yoon, T. J.; Figueiredo, J. L.; Swirski, F. K.; Weissleder, R. Rapid Detection and Profiling of Cancer Cells in Fine-Needle Aspirates. *Proc. Natl. Acad. Sci. U.S.A.* **2009**, *106*, 12459–12464.